Design of bacterially expressed influenza stem immunogens displayed on Msdps2 protein nanoparticles

Uddipan Kar[1,2], Priyanka Garg[1], Sara Khaleeq[1], Venkada Subramanian Vignesh[1], Aditya Upadhyaya[3], Mili Das[3], Suman Pandey[3], Somnath Dutta[1], Raghavan Varadarajan[1,4] *

[1] Molecular Biophysics Unit (MBU), Indian Institute of Science, Bengaluru, India

[2] Massachusetts Institute of Technology, USA, Cambridge

[3] Mynvax Private Limited, ES12, Entrepreneurship centre, SID, Indian Institute of Science, Bengaluru, India

[4] Jawaharlal Nehru Centre for Advanced Scientific Research, Jakkur, Bengaluru, India

* Corresponding Author:

Raghavan Varadarajan, Molecular Biophysics Unit, Indian Institute of Science, Bangalore, 560012 (India), Email: varadar@iisc.ac.in, PHONE: + 91-80-22932612, FAX: +91-80-23600535

Key words:

Protein design and stabilization, nanoparticle vaccine, cryo-EM studies, antibody response.

Abstract:

Influenza is a highly contagious virus, belonging to the family *Orthomyxovirus* that causes acute febrile respiratory illness which may even be fatal in some cases. Self-assembling protein nanoparticles have been used to display several copies of an immunogen, thus enhancing B cell and T cell immune responses through avidity effects. Using an iterative structure-guided approach, we successfully displayed twelve copies of a previously designed influenza stem domain immunogen pH1HA10 on the ferritin like protein, Msdps2. The nanoparticle fusion immunogen was well folded and bound to the influenza stem directed broadly neutralizing antibody CR6261 with very high affinity. An 8.5 angstrom Cryo-EM map of the nanoparticle fusion protein confirmed the successful design of the nanoparticle fusion immunogen. Preliminary mice immunization studies with the nanoparticle fusion construct revealed that the Msdps2-pH1HA10 fusion construct is immunogenic, this will be further evaluated in challenge studies.

Introduction

Influenza is a highly transmissible airborne human pathogen that can infect 5-10% of the worldwide population annually [1]. Based on the surface glycoproteins Hemagglutinin and Neuraminidase, the virus can be subdivided into 18 HA subtypes and 9 NA subtypes [2,3] out of which H1N1, H3N2 and an influenza B type are prevalent amongst the human population [4]. Recent reports of sporadic outbreaks of H5N1 and H7N9 strains with pandemic potential in humans are a matter of concern.[5].

Till now, vaccination is considered to be the most potent strategy to check viral spread. However, the high mutational rate of viral surface glycoproteins necessitates a constant annual update of the currently prevailing trivalent as well as quadrivalent vaccines [6]. Hence, several

strategies have been adopted to design 'universal influenza vaccine candidates' that can elicit cellular as well as humoral responses superior to those triggered by a natural infection, thus providing long-lasting and cross-strain protection [7,8].

The viral surface glycoprotein Hemagglutinin (HA) is the most important component of existing influenza vaccines.[9]. HA is expressed as a precursor trimeric HA0 which undergoes cleavage to form HA1 and HA2 to convert it into fusion a active form [10]. The globular HA head domain consisting solely of HA1, mediates binding to host cell sialic acid receptors while the stem domain mediates virus-host membrane fusion. Although initial studies indicated that the globular head domain is immunodominant and most neutralizing antibodies are directed towards the receptor binding site in the head domain [11], sequence analysis data revealed that the stem domain is much more conserved than the head domain [12,13] . Recently, several stem-specific neutralizing monoclonal antibodies have been isolated that showed cross-neutralization against diverse influenza strains [6,14–21]. This led to the idea that targeting the conserved stem domain of HA in the presence of immunodominant HA head domain may pave the way for 'universal influenza vaccine design'.

Application of nanotechnology has revolutionized vaccine design strategies in the past few decades including the identification of some self-assembling proteins that form nanoparticle well suited for antigen display and immune stimulation [22]. The major objective was to successfully display several copies of the same immunogen on a nanoparticle platform simultaneously leading to multivalent interactions between the nanoparticle immunogen and host cell B cell receptor due to avidity effects. This should lead to enhancement in immune responses, especially B cell and T cell responses as opposed to weaker effects of monovalent interaction afforded by a single recombinant antigen. The Nabel group pioneered the design strategy by displaying repetitive arrays of trimeric HA immunogens on the three-fold symmetry

axis of Ferritin, that elicited antibodies with increased breadth relative to recombinant soluble HA. The antibodies generated neutralized diverse related seasonal influenza strains but they failed to neutralize unmatched, divergent influenza strains [23]. Subsequently, several groups have utilized structure-based protein design to display different immunogens on the Ferritin nanoparticle platform [24–26].

Along with Ferritin, numerous other naturally occurring proteins have the property of self-assembly that can be utilized as a multimerization platform for antigen display. One such example is (MsDps2) (PDB-2Z90), a dodecameric DNA binding protein from stationary-phase cells of *Mycobacterium smegmatis* that has four three-fold axes of symmetry [27].

Previously, we reported the design of a headless stem domain immunogen H1HA10-Foldon based on H1N1 A/Puerto Rico/8/34 that conferred complete protection against homologous challenge and partial protection against heterologous influenza challenge in a mice model. Immunization with H1HA10-Foldon showed strong neutralization against the highly drifted strain H1N1 A/Puerto Rico/8/34 (serum IC_{50} titer $\geq$ 2622) [28]. With this background, we attempted to display pH1HA10 on Msdps2 protein nanoparticles [24–26].

The designed nanoparticle immunogen was found to be properly folded and exhibited strong binding to the stem-directed antibodies thus validating the design strategy. In addition, we obtained a cryo-EM map of Msdps2 displaying influenza stem immunogen (pH1HA10 on Msdps2 protein nanoparticles) at 8.5 Å whereas the Msdps2 core is resolved at 3.45 Å. Mouse challenge studies will be initiated shortly.

Materials and Methods

Cloning of the designs

The Msdps2-pH1HA10 construct was codon optimized for expression in bacteria and synthesized from GenScript (New Jersey, USA). The construct was cloned in the expression vector pET-28a (+) (Novagen) in between the Nde1 and Hind III sites. The synthesized plasmid was purified and restriction digestion (both single and double digest) was done to confirm the insert size. Initial small-scale protein induction revealed that Msdps2-pH1HA10 is soluble.

Expression and purification of the fusion protein Msdps2-pH1HA10

Msdps2 fused to pH1HA10 plasmid was transformed in chemically competent *E.coli* BL21(DE3) cells. A single sequence confirmed colony from the transformed plate was first inoculated in 50 mL of primary culture and grown overnight at 37 ^{o}C. This was followed by secondary inoculation of 1% of primary culture in 2L Terrific Broth media (Himedia) which was then grown for 4 hours at 37 ^{o}C till an OD_{600} of 0.6-0.8 was reached. The culture was then induced with 1mM IPTG. After inducing the cells for 12-16 hours at 20°C, the cells were harvested through centrifugation at 4000 rpm, 4 ^{o}C for 15 minutes, followed by sonication in 20mM Tris (pH 8.0). A second round of centrifugation at 14,000 rpm, 4 ^{o}C for 45 minutes, was then carried out to separate the soluble fraction from the insoluble fraction of the cell lysate. The soluble fraction was then allowed to bind to Ni-NTA resin (GE Healthcare Life Sciences, Amersham) at 4 ^{o}C and eluted in a gradient of imidazole (100mM, 200mM, 300mM, and 500mM) in 20mM Tris (pH 8.0). The proteins were dialysed against 2L of 20mM Tris (pH 8.0) five times at 4 ^{o}C, concentrated, aliquoted, and stored at -20 ^{o}C.

Circular Dichroism

Data acquisition was done at 298K. The spectrum was recorded on a JASCO J-715 spectropolarimeter with a protein concentration of 1-5μM in 20mM Tris (pH 8.0). The measurement was done with a 0.1 cm path length quartz cuvette by performing the scan from 260 nm to 200 nm with a response time of 4 seconds, spectral bandwidth of 2 nm, and scan rate of 50 nm/min. The final spectrum was buffer corrected. Finally mean residue ellipticity (MRE) was calculated as described [29].

Size exclusion chromatography

In order to determine the oligomeric status of the purified fusion protein, size exclusion chromatography (SEC) was performed in non-denaturing conditions. 250μg of the protein was loaded on an analytical Superdex-200 (S-200) column (GE Healthcare) and eluted in 20mM Tris (pH 8.0) at 0.5 mL/min flow rate. A low molecular weight gel filtration calibration kit (product code-28403841) (GE Healthcare) was used for calibrating the column.

Binding affinity studies by Surface Plasmon Resonance (SPR)

The binding affinity of Msdps2-pH1HA10 (Msdps2 nanoparticle fused to pH1HA10) to the stem-directed broadly neutralizing antibody (bnAb) CR6261 was measured by SPR studies performed with a Biacore 2000 optical biosensor (Biacore, Uppsala, Sweden) at 20 ^{o}C. Immobilization of the ligand, the stem-directed antibody CR6261 was carried out on a research grade CM5 chip (GE HealthCare, Uppsala, Sweden) until 700 response units were immobilized. Ovalbumin was immobilized on one sensor channel as a negative control. The analyte, nanoparticle fusion constructs were passed in a concentration series over ligand immobilized sensor channels in PBS (pH 7.4) with 0.05% P20 surfactant. A flow rate of 30μl/min was maintained throughout the binding interactions. The sensor surface was regenerated after use for successive experiments by passing 4 M magnesium chloride over the

chip surface. The final trace was corrected for non-specific binding through subtraction of the interaction signal from the ligand-free negative control channel. The data was processed and global fitting with a simple 1:1 Langmuir interaction model was done using BIA-evaluation 3.0.1 software to obtain the kinetic parameters.

Binding affinity studies by Microscale Thermophoresis (MST)

Microscale Thermophoresis was performed to detect the strengths of biomolecular interactions at minimal concentrations [30,31]. In this assay, bnAb CR6261was labelled using a Monolith™ Protein Labelling Kit RED-NHS (Catalogue Number- MO-LO11) (Nano Temper Technologies) in the supplied labelling buffer as per instructions in the manufacturer's manual. Following that, the protein was eluted into an assay buffer for MST (specifically buffer A including 0.05% Tween 20). Non-fluorescent immunogens with concentrations ranging between 5µM and 1pM were titrated in a ten-fold dilution series and mixed with a fixed amount of labelled Ab here CR6261. Next, MST Premium Coated (NanoTemper Technologies) Monolith™ NT.115 capillaries were loaded with the samples and measurement was done with the help of Monolith NT.115 and MO. Control software at room temperature at different power intensities (LED/excitation power setting 80%, MST power setting medium and high). Finally, MO.Affinity Analysis software (version 2.2.5, NanoTemper Technologies) was used to analyze the data [32].

Negative stain single particle EM

All the negative stain EM samples were prepared using staining methods described in previous studies [33,34]. Initially, glow discharge of the copper grids was carried out for 40-60 seconds at 20 mA current using GloQube glow discharge system (Quorum technologies) for uniform settling of the particles on the grid. Following this, 3.5 µl of nanoparticle (0.4 mg/mL) in 20mM Tris was adsorbed on the grids for 30-60 secs. Excess buffer was removed by blotting with a

filter paper and negative stain was performed using 1% uranyl acetate. Negative stain imaging experiment was carried out at room temperature using a FEI Tecnai 12 BioTwin transmission electron microscope equipped with a LaB6 (lanthanum hexaboride crystal) filament at a voltage of 120 Kv. Datasets were collected using a side-mounted Olympus VELITA (2Kx2K) CCD camera at a calibrated magnification of 75000 x and a defocus value of −1.3µm. The final images were recorded at a pixel size of 2.54 Å on the specimen level. Following this, properly sized particles were manually chosen and extracted using e2boxer.py and e2projectmanager.py EMAN 2.1 software [35]. Finally, a 2-D reference free classification of particles was carried out using e2refine2d.py.

Cryo-EM sample preparation and data acquisition:

Quantifoil R2/1 or R1.2/1.3 300 mesh holey carbon grids were glow discharged for 2 minutes at 20mA. The freshly prepared 3µl protein samples at a concentration of 0.5 mg/ml were added to the carbon grids and incubated for 10 seconds before plunging into liquid ethane using FEI Vitrobot Mark IV plunger at 20°C with 100% humidity. The grids were blotted for 3-5 seconds at zero blot force. Cryo-EM data acquisition of the frozen sample was carried out using a Thermo Scientific™ Talos Arctica transmission electron microscope at 200 kV at a nominal magnification of 42,200 x, equipped with a K2 Summit Direct Electron Detector. LatitudeS automatic data collection software (Gatan Inc) was utilized to collect the final 746 digital micrographs at a pixel size of 1.2 Å with a total electron dose of about 40 e-/Å^2 at the defocus range of −1.25 and −3.5 µm, under a calibrated dose of about 2 e-/Å^2 per frame. Movies were recorded for 8 secs with 20 frames. All the collected micrographs were then motion corrected using "dosefgpu_driftcorr" using MotionCor2 software [36].

Cryo-EM data processing and 3-D reconstruction

Relion 3.0 was mainly used to process the whole dataset [37,38]. The beam-induced motion correction of the individual movies was performed using MotionCor2 software. Following this, cisTEM software package [35] was used to determine the quality of the motion corrected micrographs. The contrast transfer function (CTF) correction was carried out using CTFFIND4 [39]. A total of 4,29,709 particles were automatically selected using the Relion auto-picking. The full data set was binned by 2X (2.4 Å) for reference-free 2D classification with a box size of 256 pixels and particle diameter of 220 Å. After three rounds of 2D classification, about 3,14,457 particle projections were selected for further 3D classification. Additionally, a small dataset, around 10,000 particle projections were selected for calculation of de novo initial model. This initial model was low-pass filtered to 40 Å and 3,14,457 particle projections were selected for 3D classification with T symmetry imposed and the whole data set was split into 6 classes. For this condition, a soft-mask (220 Å) was implemented to mask out the immunogen densities. Only non-bin data (1.2 Å) was utilized to calculate the final 3D structure. The best classes with stable connection between Msdps2 core and pH1HA10 extension were merged for further refinement. The 3-D reconstruction map was further subjected to focus-based refinement to separately focus on only the Msdps2 nanoparticle core (using a tight mask of 160 Å). These particles were subjected to another round of refinement for CTF and beam tilt in RELION 3.0. Subsequent movie-refinement was followed by particle polishing for further refinement. The two unfiltered half-maps were used to calculate the resolution, and the resolution of the 3D model of Msdps2 fusion was estimated at 0.143 of Fourier shell correlation (FSC) [40].

Docking of crystal structure into the cryo-EM map of Msdps2-pH1HA10 and subsequent refinement

Initially, UCSF Chimera[41] was used to visualize the Cryo-EM map as well as the available crystal structure of Msdps2 (PDB-2Z90) [27]. pH1HA10 stem domain immunogen was modelled on the crystal structure of HA from the H1N1 A/California/04/2009 strain (PDB-3LZG) [42]. The modelled structure of pH1HA10 stem domain immunogen as well as the coordinates of Msdps2 protein crystal structure (PDB-2Z90) were manually fit into the cryo-EM map of Msdps2-pH1HA10 using the "fit in Map" command of UCSF Chimera. The final docking was performed using the automatic fitting option of the UCSF Chimera visualization package.

Immunization studies in Mice

All the immunization experiments were carried out at Mynvax Pvt. Ltd, India (Study site: Vittartha LLP, Bommasandra). At zero-weeks (prime), female BALB/c mice (5 per group) were vaccinated intramuscularly with 20µg of nanoparticle vaccines mixed with AddaVax adjuvant and in a 1:1 ratio, and pre-immune sera was collected. After an interval of 4 weeks, the mice were boosted intramuscularly with 20µg of nanoparticle vaccines along with AddaVax used as adjuvant. Then, at an interval of 2 weeks, the post immune sera were collected, and an ELISA study was carried out to measure the antibody titres against the HA stem. The immunization study performed was approved by Institutional Animal Ethics Committee (IAEC) No. VIAEC/P0014/2018.

ELISA studies

ELISA was carried out with the post immune nanoparticle sera to determine the immune response. All the constructs were buffer exchanged in 1X PBS before performing the ELISA experiment. pH1HA10 protein (3µg/ml) was coated on 96-well Nunc plates (Thermo Fisher Scientific, Rochester, NY) in 50µl PBS at 4°C overnight. After washing the plates with PBST (PBS having 0.05%Tween-20), they were blocked using 3% skim milk and incubated for 2 hours. The nanoparticle sera were then diluted in a four-fold dilution series and 100µl of each

dilution was added to each well. Following 2h of incubation at room temperature, the plates were again washed with PBST. Next, 50µl of HRP-conjugated goat anti-mouse secondary antibody (Invitrogen, CA) in PBST was added at a predetermined dilution (1:5000) and incubated at room temperature for 1h. Following a final round of wash with PBST, the wells were developed with 100µl per well of the substrate 3,3′,5,5′-tetramethylbenzidine (TMB) solution (Virolabs, VA) and kept for 5 mins and OD at 450nm was calculated.

Results

Designs of Msdps2-pH1HA10 nanoparticle immunogen

Recent advancements in structural biology and lack of 'universal Influenza vaccines' have steered the attention of modern-day scientists towards self-assembling protein nanoparticles that possess the ability to display multiple copies of viral antigens in a regular repetitive manner which can mimic the geometric patterns observed for viral proteins. Multi-component nanoparticle platforms activate the adaptive immune system by stimulating B and T cell responses [43,44]. Previously, the Nabel group successfully displayed trimeric influenza immunogens on Ferritin nanoparticles which induced neutralizing antibodies [23]. Using a similar approach, we attempted to utilize an iterative structure-guided design strategy to display the previously described HA stem immunogen, H1HA10-Foldon from A/California/04/2009 H1N1 (pH1HA10-Foldon) [45] on a 12-mer self-assembling protein nanoparticle platform Msdps2 (Table 1). Msdps2, foldon, and HA10 were kept collinear in the construct. Further, since geometrical constraints in 12-meric Msdps2 enforce three-fold symmetry, the trimerization domain Foldon was also removed to develop Msdps2 fused to pH1HA10.

The schematics of the methodology employed to design Msdps2-pH1HA10 (Msdps2 fused to pH1HA10) is summarized in Figure 1. To begin with, PSA (percent solvent accessibility) calculation was done to measure the solvent accessibility of all residues in both the nanoparticle

involved (here Msdps2) and the immunogen (pH1HA10) based on their individual crystal structures/models [46]. PSA calculations indicated proper fusion between Msdps2 and pH1HA10 at the solvent exposed N-terminus of pH1HA10. The next step includes calculation of the linker length connecting the nanoparticle to the immunogen for feasible fusion. All the distance calculations were carried out using UCSF Chimera visualization software [41]. The distance between the solvent exposed C termini of Msdps2 is 24 Å. Similarly, the distance between N-termini of pH1HA10 is 45 Å. For proper fusion, the three-fold symmetry axis defined by the normal of the plane comprising the N termini of pH1HA10 has to be superimposed on the corresponding three-fold symmetry axis defined by the normal to the plane comprising the C-termini of Msdps2. In such a case, the shortest distance between the N-terminus of pH1HA10 and C terminus of Msdps2 is 12 Å, if all termini are co-planar. However, this type of fusion may lead to significant steric clashes between the two proteins. In order to avoid such steric repulsion, pH1HA10 has to be raised to a certain height above the plane formed by the Msdps2 C termini proximal to the three-fold symmetry axis and the new linker length is defined by the hypotenuse (Figure 2) which was calculated to be about 22 Å. Hence, a linker consisting of nine residues (GSAGSAGAS) was used to connect the immunogen to the nanoparticle platform. The final model of Msdps2-pH1HA10 is shown in Figure 2.

Purification and biophysical characterization of designed Msdps2-pH1HA10 nanoparticles

Msdps2-pH1HA10 fusion protein was purified from the soluble fraction of the cell lysate using Ni-NTA resin. Purified Msdps2-pH1HA10 (without Foldon) did not show any aggregate formation throughout the protein purification procedure. The final yield was 3 mg/L for Msdps2-pH1HA10 (Figure 3A). Purification with Msdps2-pH1HA10-Foldon lead to high molecular aggregate formation. So, Msdps2-pH1HA10-Foldon was not characterized further.

Following purification, the nanoparticle fused protein i.e. Msdps2-pH1HA10 was biophysically characterized. The far-UV CD spectra of the Msdps2-pH1HA10 fusion protein showed double-maxima at 208 nm and 220 nm, a characteristic signature of an alpha helix (Figure 3C). This observation was consistent with the alpha helical nature of the Msdps2 nanoparticle as observed from the crystal structure reported previously [27]. Formation of the proper self-assembly of the nanoparticle fusion, degree of oligomerization, homogeneity, and conformational heterogeneity of the designed nanoparticle fusion protein was confirmed by analytical size exclusion chromatography (SEC) (Figure 3B) under native conditions as well as negative staining TEM imaging at room temperature (Figure 3D). EM images and 2D reference free class averages of Msdps2-pH1HA10 indicated a uniform spherical particle distribution, which closely resembles the core Msdps2 nanoparticle alone. This data suggests that fusion to the influenza immunogen does not alter the overall morphology of the Msdps2 nanoparticle core. However, the displayed pH1HA10 immunogens on the nanoparticle are not noticeable in negative staining TEM images (Figure 3D). One plausible explanation can be that the flexible nature of the linker connecting the immunogen to the nanoparticle is averaged out during the 2D classification (Figure 3D) making the immunogen apparently invisible. The size of the immunogen is comparatively smaller than the core, which also allows to average out small immunogen densities from the core in 2D class averages. However, negative stain studies indicate that the Msdps2-pH1HA10 complexes are monodispersed, stable and the overall concentration is sufficient for cryo-EM studies, which finally revealed the displayed immunogen on the Msdps2 nanoparticles.

Antigenic characterization of designed Msdps2-pH1HA10 nanoparticles:

High affinity binding to conformation-specific antibodies is a useful criterion to characterize the antigenicity of the designed immunogens prior to animal immunizations. In this study, the

stem-directed broadly neutralizing antibody (bnAb) CR6261 antibody was used for all the binding studies. Surface plasmon resonance (SPR) was used to confirm the functionality of the nanoparticle immunogen Msdps2-pH1HA10 by probing its binding affinity against the CR6261antibody. The nanoparticle fusion construct bound to the antibody with very high affinity (Figure 4A). The equilibrium dissociation constant (KD) of binding of Msdps2-pH1HA10 to CR6261 antibody was about 0.7nM in SPR (Table 2). The equilibrium dissociation constant of the Msdps2 nanoparticle displaying the influenza immunogen is 10 times higher than that observed for influenza immunogen alone [45]. This clearly indicates that Msdps2-pH1HA10 fusion protein successfully displays pH1HA10 stem immunogen in its native conformation.

For cross validation, the binding affinity of the nanoparticle fusion construct to CR6261 antibody was carried out using Microscale thermophoresis (MST) (Figure 4B) and K_D's obtained were in reasonable agreement with SPR (Table 2).

Structural elucidation of designed Msdps2-pH1HA10 nanoparticles:

Our negative staining EM data clearly indicates that Msdps2-pH1HA10 particles adopt a stable oligomer, where four trimeric Msdps2 units are arranged to form a stable core with three-fold axis symmetry. In the recent past, several research groups have focused their attention towards self-assembling protein nanoparticles like Ferritin that can exhibit multivalent immunogen display leading to heightened immune response. Msdps2 is considered to be a member of the Ferritin superfamily that comprises of multi-subunit cage like proteins with a hollow interior. So, Msdps2 is structurally similar to ferritin nanoparticles, except this dps protein is expressed in *Mycobacterium smegmatis*. The present study is the first report that suggests that Msdps2 nanoparticles can successfully act as a multivalent immunogen display platform, which is able to scaffold a trimeric pH1HA10 immunogen close to the three-fold axis symmetry on Msdps2

core. Structural elucidation of the fusion nanoparticle immunogen, Msdps2-pH1HA10 is important to understand how the immunogen is displayed on the Msdps2 core as well as to probe the antibody interaction with the pH1HA10 antigen which is essential for vaccine design. The pH1HA10 immunogen displayed on the Msdps2 core was undetectable in the negative staining TEM images and class averages due to the flexible nature of linker. In order to detect the pH1HA10 immunogen on the Msdps2 nanoparticle core, we carried out cryo-EM. The micrographs and reference free 2D classifications indicate that the Msdps2-pH1HA10 particles are monodispersed and pH1HA10 immunogen was detectable in many 2D class averages (Figure 5A). These results motivated us to determine the cryo-EM structure of the Msdps2-pH1HA10 nanoparticle. Initially, 2-3 rounds of reference free 2D classification was performed on the cryo-EM dataset to remove disordered, beam damaged particles and ice contaminations. A clean dataset was used to perform 3D classification of Msdps2-pH1HA10 using a 220 Å particle diameter to separate the various conformations of the pH1HA10 extension. A spherical ball-like initial model was used without any extension for 3D classification. Interestingly, all the classes in 3D classification show four large densities sticking out from a ball-like core particle. These four large densities appear at the same position as the three-fold axis symmetry of the core Msdps2 particle. Thus, these four large elongated densities are pH1HA10 extensions, connected with the ball-like Msdps2 core structure (Figure 5B). This indicates that the majority of the Msdps2 core is attached with pH1HA10. However, some classes (class 01, class 02, and class 03) show a week connection between Msdps2 core and pH1HA10. These weak connections between core and pH1HA10 is likely due to the inherent flexibility of the linker connecting the Msdps2 core and pH1HA10. This structural characterization and 3D classification confirmed the proper display of immunogen projections on the Msdps2 nanoparticle in all eight classes.

Finally, stable classes were selected for 3D reconstruction, and the 3D structure was calculated at a resolution of 8.5 Å. Overall structural features of final 3D reconstruction are very similar with stable 3D classes (class 04, class 05, class 06, class 07, and class 08), where four clear extensions at three-fold axis symmetry of the Msdps2 core are visible. Furthermore, the available crystal structure of Msdps2 core (PDB id-2Z90) and computationally generated pH1HA10 structure was manually fit into the cryo-EM density map, and the overall fitting of the atomic model strongly supports the moderate-resolution cryo-EM map. Further, the modelled dimensions of the pH1HA10 extension and available Msdps2 crystal structure sum up to the dimensions of the 3-D cryo-EM map of Msdps2-pH1HA10 thus verifying the design (Figure 6 A-C). Due to the internal flexibility of the flexible linker between pH1HA10 and Msdps2, we are unable to resolve a near-atomic resolution structure of the Msdps2-pH1HA10 nanoparticles (Figure 6 D-E). We also performed focused refinement of the core region of the Mspdp2-pH1HA10 nanoparticle to resolve the high-resolution structure of core region (Figure 7 A-B). After CTF refinement and beam tilt correction, we are able to resolve a 3.45Å cryo-EM structure of the Msdps2 core particle, confirming that our cryo-EM data is suitable for atomic resolution structural characterization of well-ordered regions of the nanoparticle. Msdps2 crystal structure (2Z90) is fitted in cryo-EM map of Msdps2 core (Figure 7C). Additionally, all the side chains are clearly visible in the cross-sectional view of the Msdps2 core (Figure 7D). In summary, these two different 3D reconstructions suggest that the Mspdp2-pH1HA10 nanoparticle with four stable extensions is characterized at 8.5 Å and the Msdps2 core at ~3.45 Å, respectively.

Immunogenicity of the designed Msdps2-pH1HA10 nanoparticle fusion in mice model

Preliminary mice immunization experiments were carried out with the nanoparticles Msdps2-pH1HA10 as well as with pH1HA10 alone without any nanoparticle display as a control

(Figure 8A). The post immune sera were collected, and ELISA was performed for both pH1HA10 alone as well as with the nanoparticle platform i.e. Msdps2-pH1HA10 against pH1HA10 (Figure 8B). For each of the titration, end point titer was calculated as the dilution that gives twice the value of pre-immune sera. End point titer values for Msdps2-pH1HA10 was 1/102400 while that for pH1HA10 was 1/102400. The 50 percent ELISA binding titer values are calculated as sera dilution that gives 50% of maximum absorbance value. The 50% ELISA binding titer values in terms of sera dilution when tested against pH1HA10 are 1/19200 for MSdps2-pH1HA10 and 1/25600 for pH1HA10 (self- titer). Although there were no notable improvement in Optical Density (OD_{450nm}) values of Msdps2-pH1HA10 as compared to pH1HA10 alone, challenge studies with Msdps2 nanoparticle are to be carried out in the future to determine the vaccine efficacy.

Discussion

Focussing the immune response to conserved epitopes on HA is a promising strategy towards the development of 'universal vaccine candidates [47–49]. This has resulted in the development of various subunit vaccine designs eliciting responses to HA head or HA stem [50].

Several recent studies have described self-assembling protein nanoparticles that induce broadly neutralizing antibody responses against influenza virus in mice and ferrets [23,24]. Using similar approaches to ours, immunogens derived from the surface proteins of HIV-1, and RSV have been displayed on self-assembling, naturally occurring nanoparticles, as well as computationally designed nanoparticle scaffolds [51,52]. Recently, there was a report of a double-layered nanoparticle that induced broad protection against divergent influenza strains [53]. Owing to the flexible nature of the displayed immunogens, it has not been possible to obtain a high resolution cryo-EM map for any nanoparticle immunogen fusion to date. In addition, all the above immunogens have been expressed in mammalian or insect cells. In contrast, in the

present case, the immunogen is bacterially expressed; which has several advantages in terms of cost and scalability.

In this work, we have successfully shown the design and structural characterization of an Msdps2 nanoparticle fusion where the stem domain subunit immunogen pH1HA10 was displayed on 12-mer Msdps2 nanoparticles. The nanoparticle fusion protein was purified in moderate yield and was properly folded. The nanoparticle fusion construct showed high affinity binding to the conformation specific stem-directed antibody CR6261, thus confirming the correct design strategy. Size exclusion analysis and negative stain EM data clearly indicate proper homogenous particle formation.

Since the immunogen extensions were not visible in negative stain images, we employed Cryo-EM to detect the antigen displayed on the nanoparticle platform. Several labs have previously carried out cryo-EM analysis of nanoparticle immunogen display platforms since a high resolution cryo-EM map is more likely to provide additional structural information on the displayed immunogens. The Cryo-EM map of the HA stem displayed on Ferritin nanoparticles was obtained at a low resolution of 16 Å [24]. In 2019, the King group solved the Cryo-EM structure of a computationally designed nanoparticle I53 displaying the Respiratory Syncytial Virus (RSV) virus at a resolution of 6.3 Å [52]. Recently, there are reports of cryo-EM maps of several computationally designed two-component protein nanoparticle immunogen display platforms at a resolution of 3.9-6.67 Å [54,55]. In most of these cryo-EM studies, the displayed immunogens were more poorly resolved than the corresponding nanoparticle core. Here, we obtained a moderate resolution cryo-EM map of a naturally occurring protein nanoparticle immunogen display platform (Msdps2 displaying influenza stem immunogen). [54,56].. Further, the immunogens (pH1HA10) in the Cryo-EM maps were displayed on the three-fold symmetry axes on the nanoparticle Msdps2 thus validating the correct design strategy. The immunogens

are attached to the Msdps2 nanoparticle core by 9 amino acid linker (GSAGSAGAS) as mentioned before in Result section. GS (Gly Ser) linkers are considered to be one of the most widely used flexible linkers in fusion protein designs owing to their small size which accounts for the mobility of the fusion proteins. Further, these linkers can form hydrogen bonds in an aqueous solution which provides additional stability to the linkers avoiding unnecessary interaction with the fusion protein [57,58]. A plausible reason for the moderate cryo-EM resolution obtained in the study is this flexible nature of the displayed immunogen which may lead to distortion of global alignment thus hampering the overall resolution of the Msdps2-pH1HA10 fusion protein. Alternative linker designs to decrease the flexibility of the displayed antigen might result in a higher resolution structure, though whether this will enhance immunogenicity in unclear. Several previous studies have indicated that flexibility of the particle does not depend on the beam-induced motion or mechanical drift. An increase in flexibility leads to relative movement of different regions of the molecule which finally reduced the quality of the final data with a single long exposure [59]. Our result is in accord with the previous cryo-EM studies of nanoparticle immunogen fusion by other labs where the 3-D reconstruction of complete nanoparticles gave rise to highly diffused and poorly resolved displayed immunogen as compared to the nanoparticle core [52,55]. Focused refinement of the Msdps2 core gave rise to a high resolution cryo-EM map of the core with a resolution of 3.45 Å. This enhancement of resolution on focused refinement confirms our hypothesis that linker flexibility is responsible for the loss of resolution in the overall cryo-EM map. The available crystal structure (PDB) was found to fit extremely well to the Cryo-EM map of the Msdps2 core. The whole Cryo-EM map generation was *de-novo* without considering any available crystal structures as a template. Till date, this is the highest resolution cryo-EM map attained with any naturally occurring protein nanoparticle immunogen fusion.

Mice immunization with the nanoparticle fusion constructs indicated that the Msdps2-pH1HA10 antigen was immunogenic, though surprisingly not much more than the previously described parent trimeric stem immunogen [45]. Influenza challenge studies in mice and ferrets are to be carried out in the near future to further validate the present results.

Author Contributions

RV and UK designed the study and analysed and interpreted most of the data. UK performed most of the biophysical characterization experiments except for some of the data in Figure 3 and Table 2 which were generated by SK and VS . SD designed the cryo-EM data collection and image processing. PG and SD carried out all the negative stain EM and cryo-EM data processing, data analysis and data interpretation. AU did some of the protein purifications, MD did the ELISA assays. SP formulated the immunogens and coordinated the animal immunizations. UK, SD and RV wrote the manuscript.

Acknowledgements

We thank Prof Dipankar Chatterji (Molecular Biophysics Unit, IISc) for providing us with the Msdps2 plasmid. We acknowledge technical support from Ms. Srilatha for assistance during SPR experiments. We sincerely acknowledge funding from DST, UAY, and UGC-CSIR doctoral fellowship. We acknowledge financial supports from the Science and Engineering Research Board (SERB) (Grant No-SB/S2/RJN-145/2015) and DBT (Grant No-BT/PR25580/BRB/10/1619/2017) for cryo-EM consumables and computer cluster for image processing. We are also thankful to Department of Biotechnology (BT/INF/22/SP22844/2017) and DST-FIST (SR/FST/LSII-039/2015) for National cryo-EM facility at IISc and DBT-IISc

partnership program phase II for negative stain TEM facility at Biological Sciences Division, IISc.

Conflict of Interest

The authors declare no competing financial interests.

References

1. Reed, C. *et al.* Estimates of the prevalence of pandemic (H1N1) 2009, United States, April-July 2009. *Emerg. Infect. Dis.* **15**, 2004–7 (2009).

2. Tong, S. *et al.* New world bats harbor diverse influenza A viruses. *PLoS Pathog.* **9**, e1003657 (2013).

3. Shi, Y., Wu, Y., Zhang, W., Qi, J. & Gao, G. F. Enabling the 'host jump': Structural determinants of receptor-binding specificity in influenza A viruses. *Nature Reviews Microbiology* **12(12)**, 822-31 (2014).

4. Girard, M. P., Cherian, T., Pervikov, Y. & Kieny, M. P. A review of vaccine research and development: Human acute respiratory infections. *Vaccine* **23(50)**, 5708-24 (2005).

5. Belser, J. A. *et al.* Pathogenesis of avian influenza (H7) virus infection in mice and ferrets: enhanced virulence of Eurasian H7N7 viruses isolated from humans. *J. Virol.* **81**, 11139–47 (2007).

6. Pica, N. & Palese, P. Toward a universal influenza virus vaccine: prospects and challenges. *Annu. Rev. Med.* **64**, 189–202 (2013).

7. Berlanda Scorza, F., Tsvetnitsky, V. & Donnelly, J. J. Universal influenza vaccines:

Shifting to better vaccines. *Vaccine* **34(26)**, 2926-2933 (2016).

8. Paules, C. I., Marston, H. D., Eisinger, R. W., Baltimore, D. & Fauci, A. S. The Pathway to a Universal Influenza Vaccine. in *Immunity* **47(4)**, 599-603 (2017).

9. Safdar, A. & Cox, M. M. J. Baculovirus-expressed influenza vaccine. A novel technology for safe and expeditious vaccine production for human use. *Expert Opin. Investig. Drugs* **16**, 927–34 (2007).

10. Skehel, J. J. & Wiley, D. C. Receptor Binding and Membrane Fusion in Virus Entry: The Influenza Hemagglutinin. *Annu. Rev. Biochem.* **69**, 531-69 (2000).

11. Wiley, D. C., Wilson, I. A. & Skehel, J. J. Structural identification of the antibody-binding sites of Hong Kong influenza haemagglutinin and their involvement in antigenic variation. *Nature* **289(5796)**, 373-8 (1981). doi:10.1038/289373a0

12. Both, G. W., Sleigh, M. J., Cox, N. J. & Kendal, A. P. Antigenic drift in influenza virus H3 hemagglutinin from 1968 to 1980: multiple evolutionary pathways and sequential amino acid changes at key antigenic sites. *J. Virol.* **48(1)**, 52-60 (1983).

13. Nobusawa, E. *et al.* Comparison of complete amino acid sequences and receptor-binding properties among 13 serotypes of hemagglutinins of influenza A viruses. *Virology* **182**, 475–485 (1991).

14. Corti, D. *et al.* A neutralizing antibody selected from plasma cells that binds to group 1 and group 2 influenza A hemagglutinins. *Science* **333**, 850–6 (2011).

15. Ekiert, D. C. *et al.* Antibody recognition of a highly conserved influenza virus epitope. *Science* **324**, 5924 (2009).

16. Krammer, F. & Palese, P. Influenza virus hemagglutinin stalk-based antibodies and vaccines. *Curr. Opin. Virol.* **3**, 521–30 (2013).

17. Ekiert, D. C. *et al.* A highly conserved neutralizing epitope on group 2 influenza A viruses. *Science* **333**, 843-50 (2011).

18. Okuno, Y., Isegawa, Y., Sasao, F. & Ueda, S. A common neutralizing epitope conserved between the hemagglutinins of influenza A virus H1 and H2 strains. *J. Virol.* **67(5)**, 2552-8 (1993).

19. Sanchez-Fauquier, A., Guillen, M., Martin, J., Kendal, A. P. & Melero, J. A. Conservation of epitopes recognized by monoclonal antibodies against the separated subunits of influenza hemagglutinin among type A viruses of the same and different subtypes. *Arch. Virol.* **116**, 285–92 (1991).

20. Throsby, M. *et al.* Heterosubtypic neutralizing monoclonal antibodies cross-protective against H5N1 and H1N1 recovered from human IgM+ memory B cells. *PLoS One* **3**, e3942 (2008).

21. Sui, J. *et al.* Structural and functional bases for broad-spectrum neutralization of avian and human influenza A viruses. *Nat. Struct. Mol. Biol.* **16**, 265–73 (2009).

22. Lee, L. A. & Wang, Q. Adaptations of nanoscale viruses and other protein cages for medical applications. *Nanomedicine* **2**, 137–49 (2006).

23. Kanekiyo, M. *et al.* Self-assembling influenza nanoparticle vaccines elicit broadly neutralizing H1N1 antibodies. *Nature* **499**, 102–106 (2013).

24. Yassine, H. M. *et al.* Hemagglutinin-stem nanoparticles generate heterosubtypic influenza protection. *Nat. Med.* **21**, 1065–1070 (2015).

25. Georgiev, I. S. *et al.* Two-Component Ferritin Nanoparticles for Multimerization of Diverse Trimeric Antigens. *ACS Infect. Dis.* **4**, 788–796 (2018).

26. Corbett, K. S. *et al.* Design of Nanoparticulate Group 2 Influenza Virus Hemagglutinin

Stem Antigens That Activate Unmutated Ancestor B Cell Receptors of Broadly Neutralizing Antibody Lineages. *MBio* **10**, (2019).

27. Roy, S., Saraswathi, R., Chatterji, D. & Vijayan, M. Structural Studies on the Second Mycobacterium smegmatis Dps: Invariant and Variable Features of Structure, Assembly and Function. *J. Mol. Biol.* **375**, 948–959 (2008).

28. Mallajosyula, V. V. A. *et al.* Influenza hemagglutinin stem-fragment immunogen elicits broadly neutralizing antibodies and confers heterologous protection. *Proc. Natl. Acad. Sci.* **111**, E2514–E2523 (2014).

29. Ganesh, C., Shah, A. N., Swaminathan, C. P., Surolia, A. & Varadarajan, R. Thermodynamic characterization of the reversible, two-state unfolding of maltose binding protein, a large two-domain protein. *Biochemistry* **36**, 5020–5028 (1997).

30. Jerabek-Willemsen, M., Wienken, C. J., Braun, D., Baaske, P. & Duhr, S. Molecular Interaction Studies Using Microscale Thermophoresis. *Assay Drug Dev. Technol.* **9**, 342–353 (2011).

31. Jerabek-Willemsen, M. *et al.* MicroScale Thermophoresis: Interaction analysis and beyond. *J. Mol. Struct.* **1077**, 101–113 (2014).

32. Wienken, C. J., Baaske, P., Rothbauer, U., Braun, D. & Duhr, S. Protein-binding assays in biological liquids using microscale thermophoresis. *Nat. Commun.* **1**, 1–7 (2010).

33. Kumar, S. *et al.* An HIV-1 Broadly Neutralizing Antibody from a Clade C-Infected Pediatric Elite Neutralizer Potently Neutralizes the Contemporaneous and Autologous Evolving Viruses. *J. Virol.* **93(4)**, e01495 (2018). doi:10.1128/jvi.01495-18

34. Ghosh, E. *et al.* Conformational Sensors and Domain Swapping Reveal Structural and Functional Differences between β-Arrestin Isoforms. *Cell Rep.* **28(13)**, 3287-3299 (2019).

35. Bell, J. M., Chen, M., Baldwin, P. R. & Ludtke, S. J. High resolution single particle refinement in EMAN2.1. *Methods* **100**, 25–34 (2016).

36. Zheng, S. Q. *et al.* MotionCor2: Anisotropic correction of beam-induced motion for improved cryo-electron microscopy. *Nat. Methods* **14**, 331–332 (2017).

37. Scheres, S. H. W. RELION: Implementation of a Bayesian approach to cryo-EM structure determination. *J. Struct. Biol.* **180**, 519–530 (2012).

38. Kimanius, D., Forsberg, B. O., Scheres, S. H. W. & Lindahl, E. Accelerated cryo-EM structure determination with parallelisation using GPUS in RELION-2. *Elife* **5**, 1–21 (2016).

39. Rohou, A. & Grigorieff, N. CTFFIND4: Fast and accurate defocus estimation from electron micrographs. *J. Struct. Biol.* 192(2), 216-21 (2015).

40. Van Heel, M. & Schatz, M. Fourier shell correlation threshold criteria. *J. Struct. Biol.* **151(3)**, 250-62 (2005).

41. Pettersen, E. F. *et al.* UCSF Chimera - A visualization system for exploratory research and analysis. *J. Comput. Chem.* **25**, 1605–1612 (2004).

42. Xu, R. *et al.* Structural basis of preexisting immunity to the 2009 H1N1 pandemic influenza virus. *Science* **328**, 357–60 (2010).

43. Bachmann, M. F. *et al.* The influence of antigen organization on B cell responsiveness. *Science* **262(5138)**, 1448-51 (1993).

44. Zhao, L. *et al.* Nanoparticle vaccines. *Vaccine* **32(3)**, 327-37 (2014).

45. Mallajosyula, V. V. A. *et al.* Influenza hemagglutinin stem-fragment immunogen elicits broadly neutralizing antibodies and confers heterologous protection. *Proc. Natl. Acad. Sci. U. S. A.* **111(25)**, E2514-23 (2014).

46. Hoskins, J., Lovell, S. & Blundell, T. L. An algorithm for predicting protein-protein interaction sites: Abnormally exposed amino acid residues and secondary structure elements. *Protein Sci.* **15**, 1017–1029 (2006).

47. Du, L., Zhou, Y. & Jiang, S. Research and development of universal influenza vaccines. *Microbes Infect.* **12**, 280–286 (2010).

48. Sui, J. *et al.* Structural and functional bases for broad-spectrum neutralization of avian and human influenza A viruses. *Nat. Struct. Mol. Biol.* **16**, 265–273 (2009).

49. Steel, J. *et al.* Influenza Virus Vaccine Based on the Conserved Hemagglutinin Stalk Domain. *MBio* **1(1)**, e00018-10 (2010).

50. Xu, R. *et al.* A recurring motif for antibody recognition of the receptor-binding site of influenza hemagglutinin. *Nat. Struct. Mol. Biol.* **20**, 363–70 (2013).

51. Jardine, J. *et al.* Rational HIV immunogen design to target specific germline B cell receptors. *Science* **340**, 711–716 (2013).

52. Marcandalli, J. *et al.* Induction of Potent Neutralizing Antibody Responses by a Designed Protein Nanoparticle Vaccine for Respiratory Syncytial Virus. *Cell* **176**, 1420-1431.e17 (2019).

53. Deng, L. *et al.* Double-layered protein nanoparticles induce broad protection against divergent influenza A viruses. *Nat. Commun.* **9(1)**, 359 (2018).

54. Ueda, G. *et al.* Tailored design of protein nanoparticle scaffolds for multivalent presentation of viral glycoprotein antigens. *Elife* **9**, e57659(2020).

55. Antanasijevic, A. *et al.* Structural and functional evaluation of de novo-designed, two-component nanoparticle carriers for HIV Env trimer immunogens. *PLoS Pathog.* **16(8)**, e1008665 (2020).

56. López-Sagaseta, J., Malito, E., Rappuoli, R. & Bottomley, M. J. Self-assembling protein nanoparticles in the design of vaccines. *Computational and Structural Biotechnology Journal* **14**, 58-68 (2016).

57. Chen, X., Zaro, J. L. & Shen, W. C. Fusion protein linkers: Property, design and functionality. *Advanced Drug Delivery Reviews* **65(10)**, 1357-69 (2013).

58. Van Rosmalen, M., Krom, M. & Merkx, M. Tuning the Flexibility of Glycine-Serine Linkers to Allow Rational Design of Multidomain Proteins. *Biochemistry* **56(50)**, 6565-6574 (2017).

59. Rawson, S., Iadanza, M. G., Ranson, N. A. & Muench, S. P. Methods to account for movement and flexibility in cryo-EM data processing. *Methods* **100***,* 35-41 (2016).

Tables:

Particle Construct	Oligomeric status	Number of pH1HA10 displayed	Particle termini involved in fusion	Linker length	Number of residues in linker	Molecular weight of fusion (KDa)
Msdps2 (PDB-2Z90)	12-mer (4 three-fold axes)	12 (4 trimers)	C terminus	22	9	415

Immunogen	Technique	Ligand	k_{on} ($M^{-1}s^{-1}$)	k_{off} (s^{-1})	K_D (nM)
Msdps2 pH1HA10	SPR	CR6261	$(5.3\pm 0.6)*10^4$	$(3.6 \pm 0.2)*10^{-5}$	0.7 ± 0.8
Msdps2 pH1HA10	MST	CR6261			1.1 ± 0.5

Table 1: Details of the nanoparticle platforms used:

Overview of Msdps2 nanoparticle platform used in the study.

Table 2: Binding parameters for interaction of Msdps2-pH1HA10 with bNAb CR6261 measured by SPR and MST

Figures:

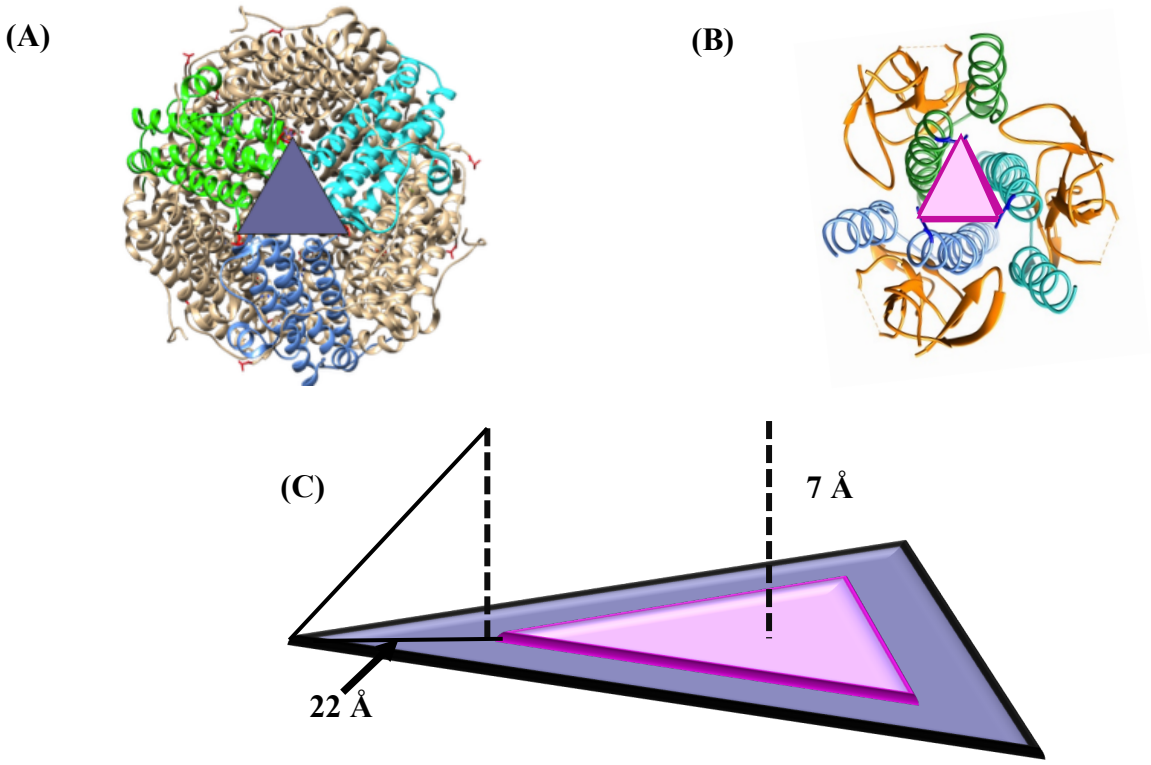

Figure 1: Design of Msdps2 nanoparticle fusion: (A) Crystal structure of Msdps2 (PDB- 2Z90) with three-fold symmetry axis perpendicular to the plane formed by the three C termini shown in violet (B) model of pH1HA10 on crystal structure of A/California/04/2009 H1N1(PDB -3LZG) with three-fold symmetry axis perpendicular to the plane formed by the three N termini shown in pink (C) superposition of the planes of C termini of Msdps2 and N termini of pH1HA10, when coplanar. To minimize steric hindrance, pH1HA10 N termini are

raised above the Msdps2 C termini by 7 Å. The shortest distance between the N termini of pH1HA10 and the C termini of Msdps2 is 22 Å.

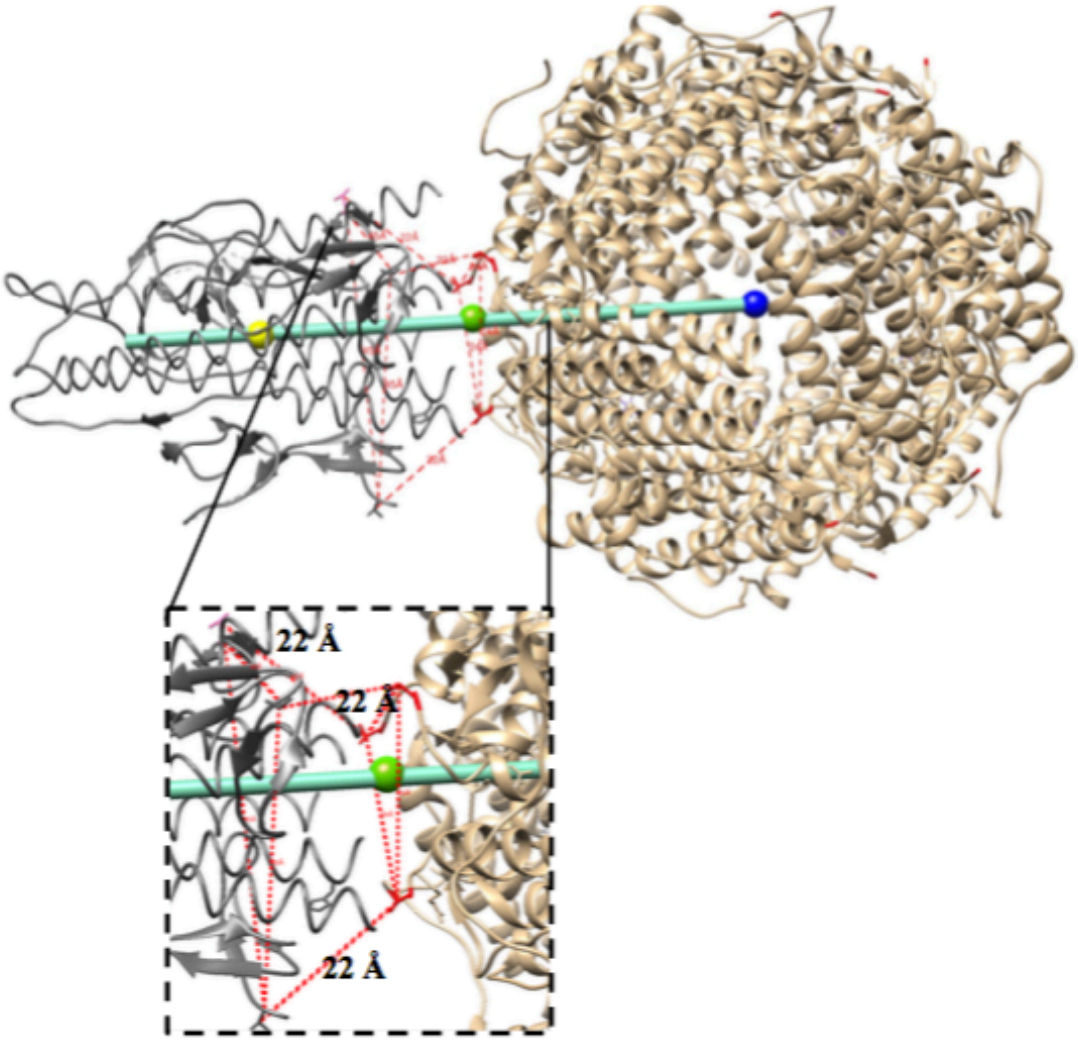

Figure 2: Model of pH1HA10 fused to Msdps2: the immunogen pH1HA10 (grey) is displayed on the Msdps2 nanoparticle (golden yellow) platform along four 3-fold axes (only one 3-fold axes is shown in the figure) while the inset shows the zoomed in view of the fusion interface. The 3-fold axes is shown in cyan. The centroid of the triangle formed by the C termini of Msdps2 (red) is shown in green. The centroids of the pH1HA10 and Msdps2 nanoparticles

are shown in yellow and blue respectively. The closest distance between the N termini of pH1HA10 and C termini of Msdps2 is 22 Å.

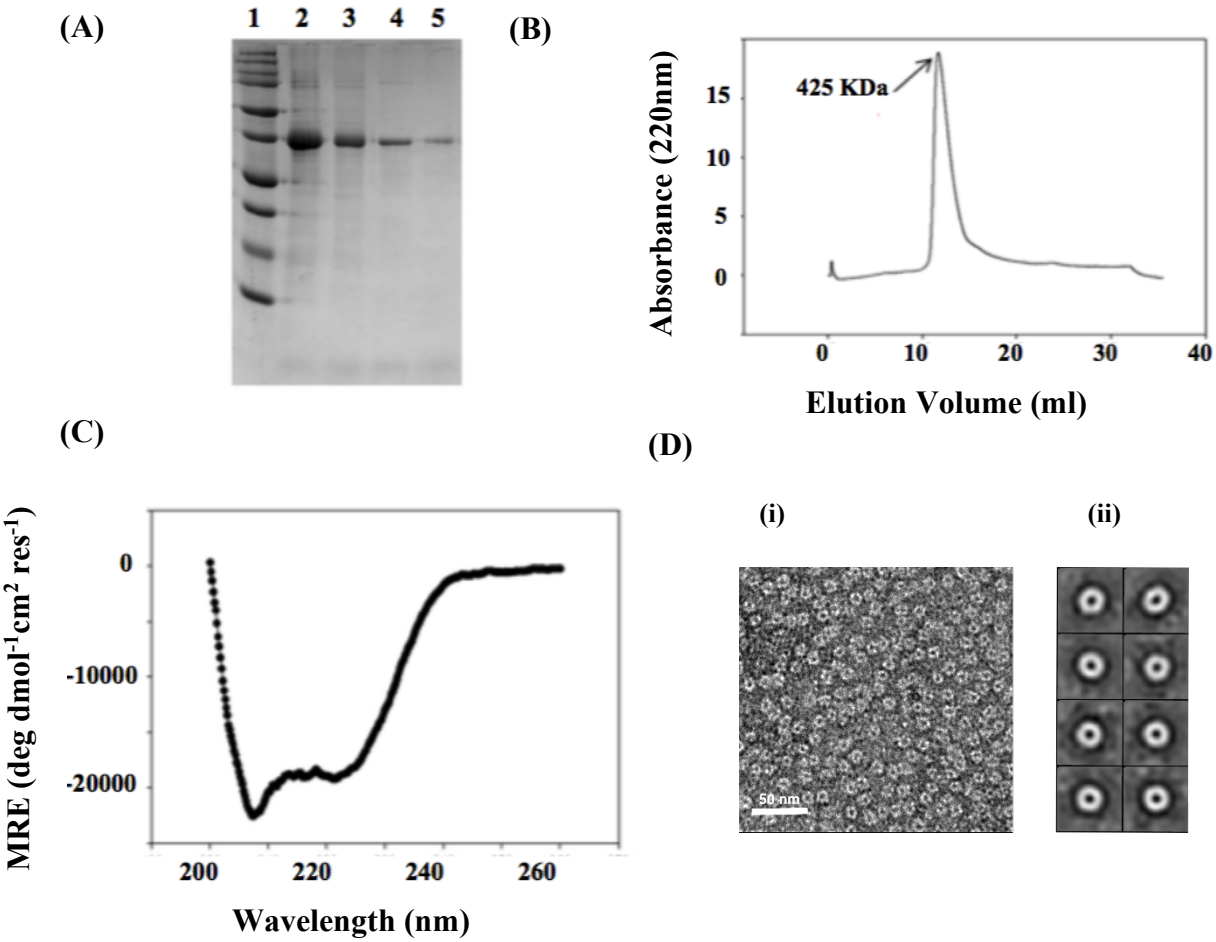

Figure 3: Biophysical characterization of pH1HA10 fused to Msdps2: (A) SDS-PAGE analysis of Msdps2-pH1HA10: Lane 1- Marker, Lane (2-5) – Msdps2-pH1HA10 elutions. Msdps2-pH1HA10 has an expected molecular weight of 34 KDa. (B) SEC profile of Msdps2-pH1HA10 with a single particle peak at the expected molecular weight of the nanoparticle fusion (425 KDa) (C) Far UV-CD spectra of Msdps2-pH1HA10 (D) Negative stain EM images of Msdps2-pH1HA10 **(i)** Micrograph of negative stain EM images for Msdps2-pH1HA10. **(ii)** 2D class averages obtained from the EM data.

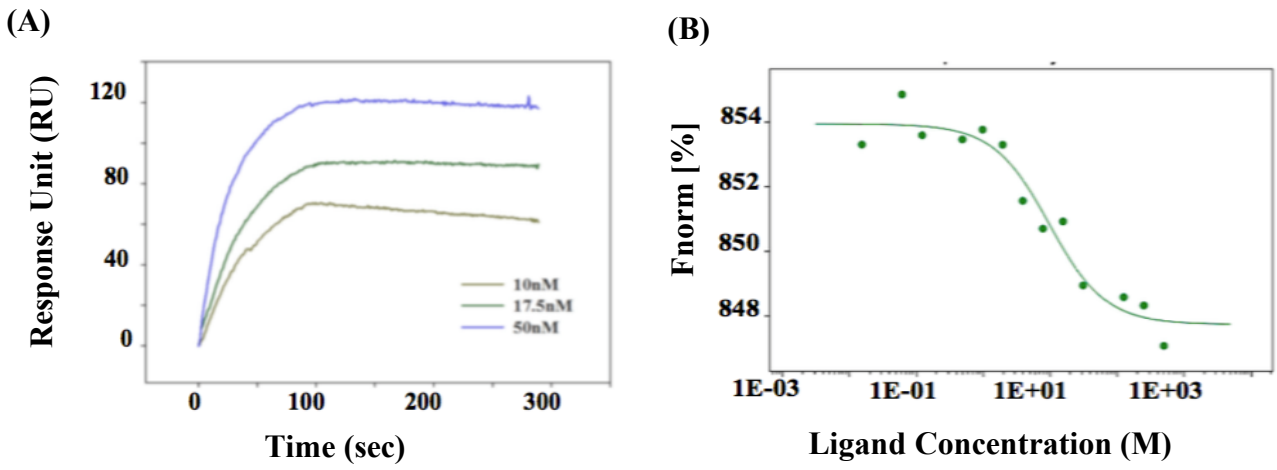

Figure 4: Antigenic characterization of designed of pH1HA10 fused to Msdps2: (A) Msdps2-pH1HA10 binds tightly to the stem directed broadly neutralizing antibody CR6261. Varying concentrations used for the binding interaction analysis by SPR. The kinetic parameters are listed in Table 2. (B) Binding measured by MST where the non-fluorescent nanoparticle fusion design Msdps2-pH1HA10 with concentrations ranging from 5 µM to 1 pM were titrated in a ten-fold dilution series and mixed with a fixed concentration of 10nM labelled Ab CR6261 in 20mM Tris buffer (pH-8.0). The normalized fluorescence F norm (ratio of MST laser on/MST laser off) is plotted as a function of concentration of ligand. Both techniques gave similar affinities of ∼1nM.

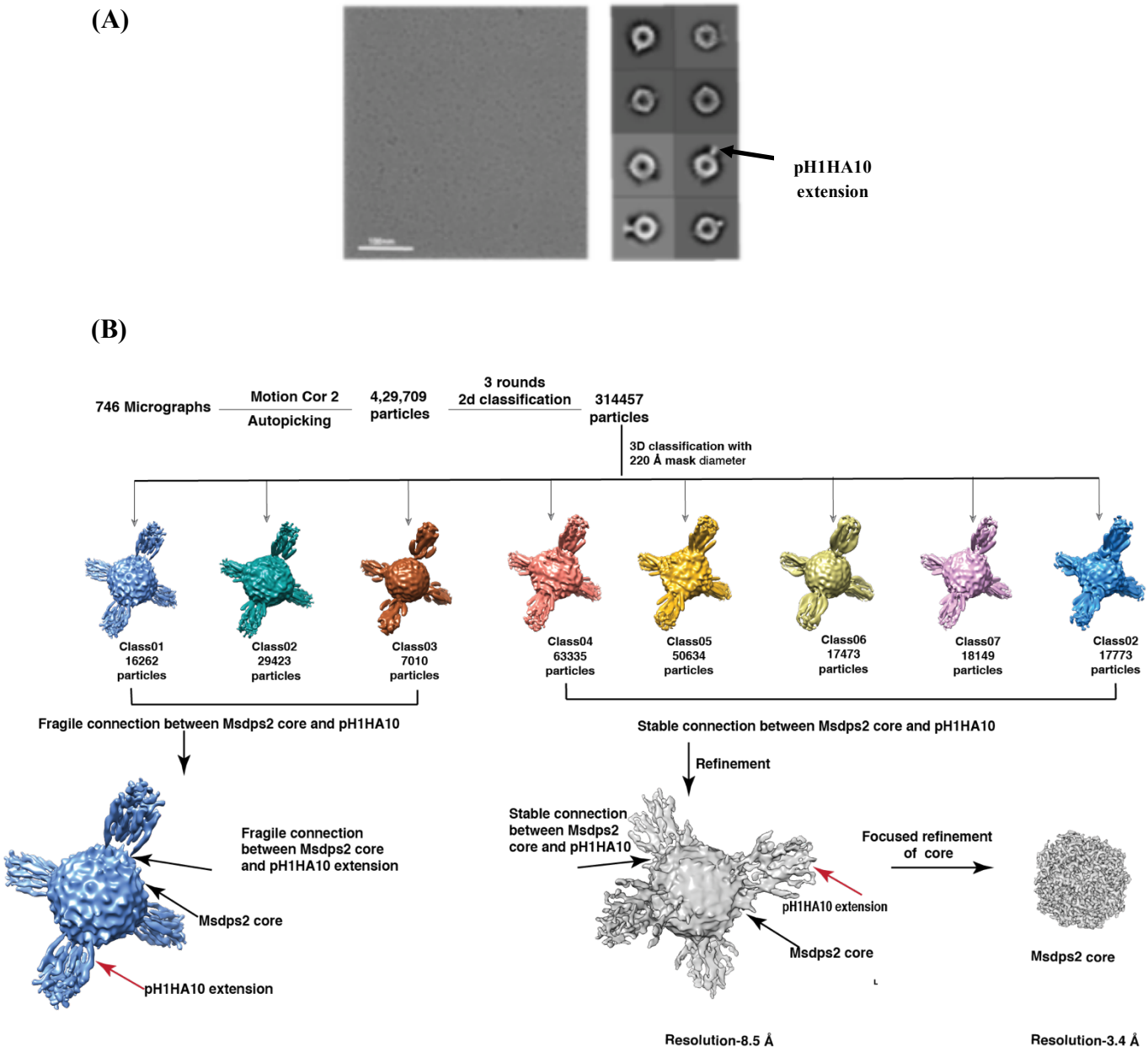

Figure 5: Cryo-EM structural elucidation of Msdsps2-pH1HA10: (A) Raw cryo-EM micrograph of Msdps2-pH1HA10 with the reference free 2D class averages of Msdps2-pH1HA10 nanoparticles. (B) Routine 3-D classification using 220Å particle diameter and 3D reconstruction of Msdps2-pH1HA10. A total of 746 micrographs were collected.

4,29,709 particles were selected after motion correction and auto picking of the data set. Three rounds of 2-D classification led to the identification of 3,14,457 distinct particles. The particles were then divided into eight classes each having different particle numbers. Classes having different connections (fragile or stable) between Msdps2 core and pH1HA10 extension were merged separately. The generated cryo-EM map obtained from the refinement of Msdps2-pH1HA10 particles with stable connections could be refined to a resolution of 8.5 Å. Focused refinement of Msdps2 core (using a tight mask of 160 Å particle diameter) lead to a near-atomic resolution of 3.4 Å.

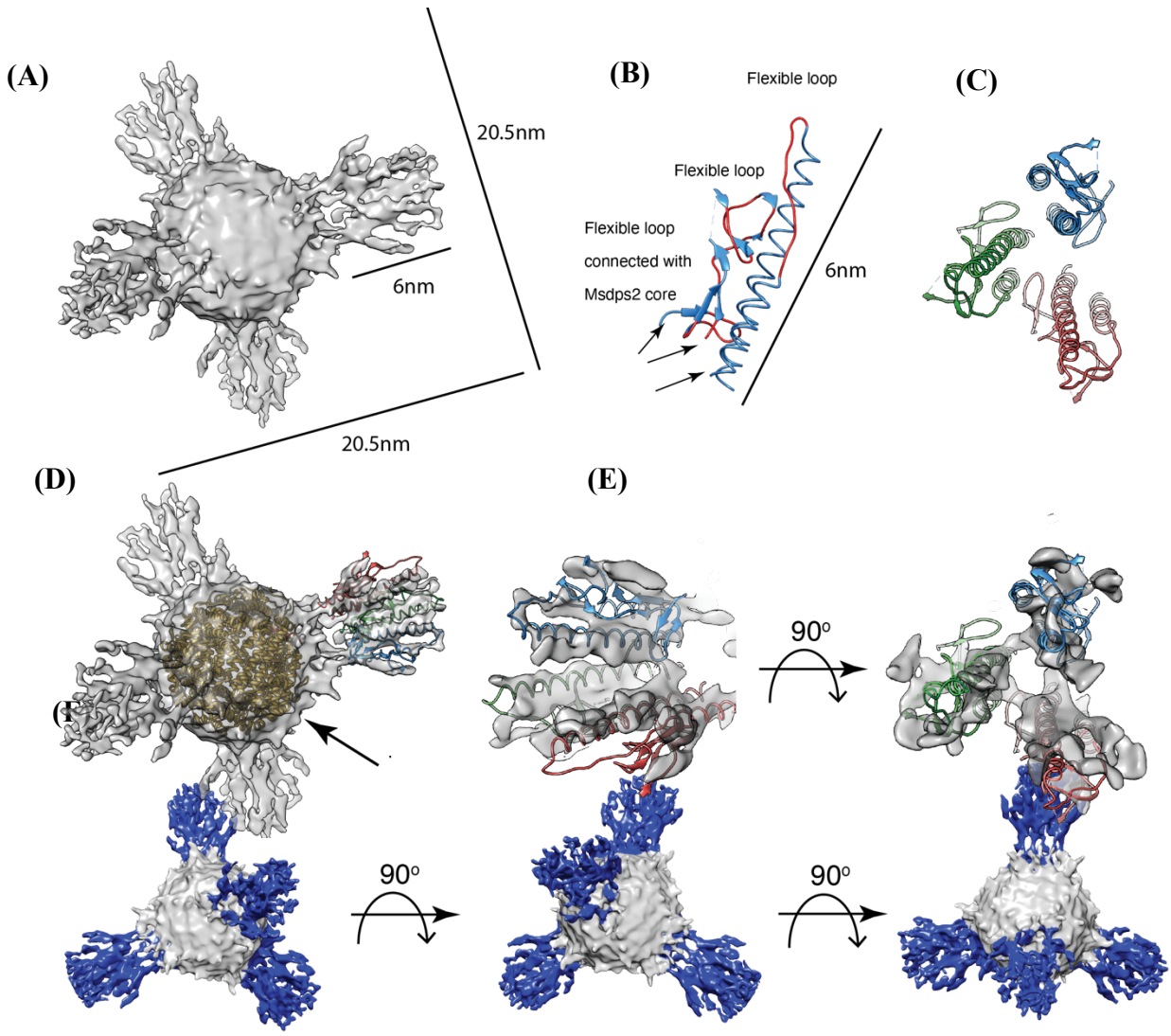

Figure 6: Fitting of cryo-EM map of Msdsps2-pH1HA10: (A) Dimensions of the refined 3-D cryo-EM map of Msdps2-pH1HA10. (B) modelled structure of pH1HA10 protomer. Flexible loops are shown in red. Dimension of pH1HA10 model structure is calculated to be 6 nm. (C) top view of modelled structure of pH1HA10 trimer. (D) Manual fit of Msdps2 crystal structure (2Z90) and modelled structure of only one pH1HA10 trimer in the cryo-EM map obtained is shown for representation. (E) Side and top view cross-section of cryo-EM map of extension alone shows fitting of pH1HA10 trimer. The protomers in pH1HA10 trimers are shown in blue, red and green respectively. Loop regions are poorly fitted

owing to loop flexibility. (F) Different views of refined 3-D cryo-EM map of Msdps2-pH1HA10. pH1HA10 extension is shown in blue.

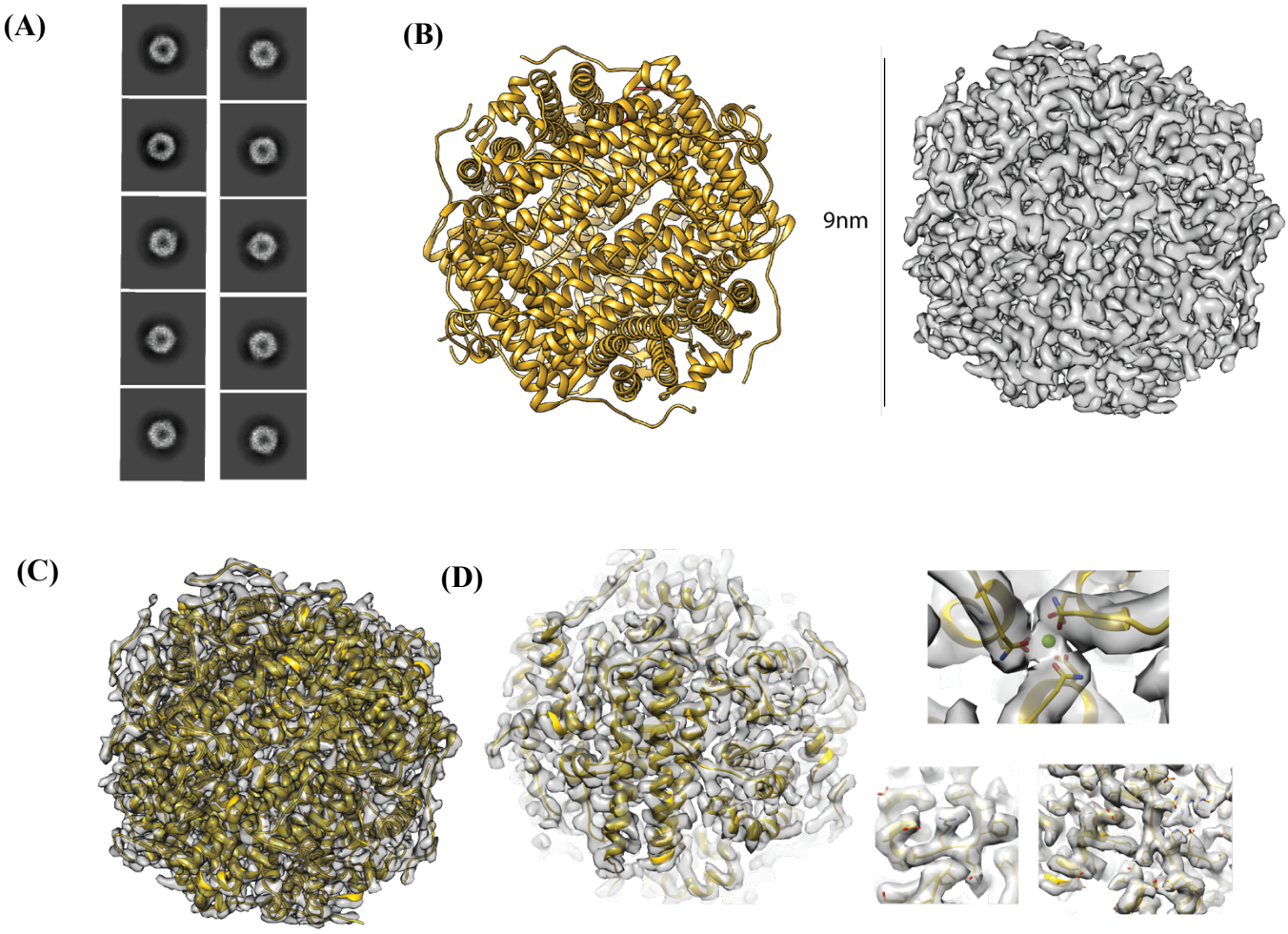

Figure 7: Fitting of cryo-EM core map (focused refinement of core) with Msdsps2 crystal structure (PDB id- 2Z90): (A) reference free 2D class averages of raw cryo-EM micrographs of Msdps2 core obtained on focused refinement (using a tight mask of 160 Å particle diameter) (B) Dimensions of crystal structure of Msdps2 (left) (PDB- 2Z90) completely match that of focused 3-D reconstruction of nanoparticle core (right). (C) Manual fitting of coordinates of Msdps2 crystal structure to focused cryo-EM map of the core. (D) Cross-sectional view reveals available crystal structure fits completely into the electron density.

(A)

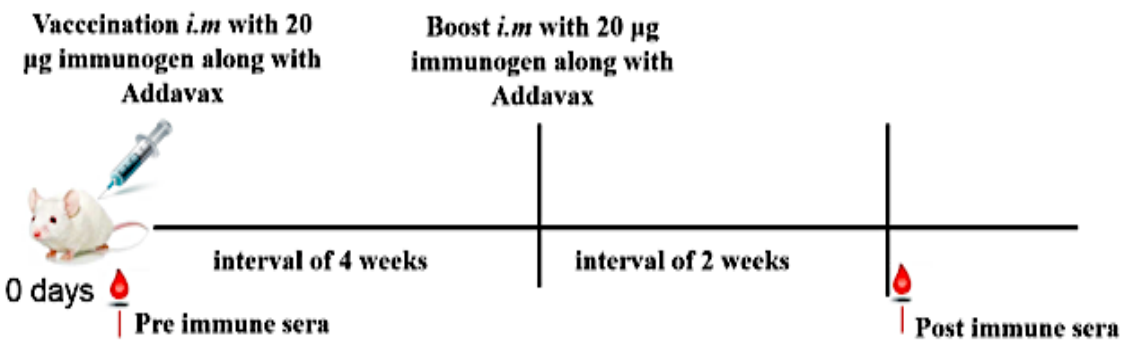

(B)

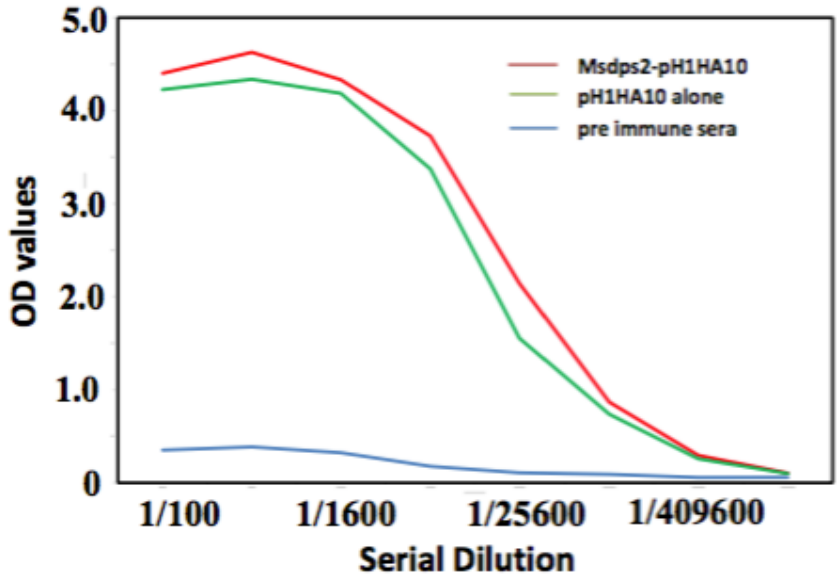

Figure 8: Mice immunization studies: (A) denotes the immunization protocol followed during the study. Mice were vaccinated with nanoparticle fused immunogen Msdps2-pH1HA10 and also pH1HA10 alone at day zero and boosted with the immunogens after an interval of 4 weeks. Finally, at an interval of two weeks after boost, post immune sera were taken and ELISA was done. Pre-immune sera were also collected as a control. (B) ELISA plot where OD_{450nm} is plotted against various sera dilution. Reported values are mean ± SD (standard deviation) values of three independent experiments. Red and green denotes values obtained with post immune sera for Msdps2-pH1HA10 and pH1HA10 alone while blue denotes the pre-immune sera value for Msdps2-pH1HA10. End point titer was calculated as the dilution that gives twice the value of pre-immune sera. End point titer values for both

constructs against pH1HA10 in terms of serum dilution are given here: Msdps2-pH1HA10- 1/102400, pH1HA10- 1/102400. The 50 percent ELISA binding titer values are calculated as sera dilution that gives 50% of maximum absorbance value. The 50% ELISA binding titer values tested against pH1HA10 in terms of sera dilution are given as: Msdps2-pH1HA10- 1/19200, pH1HA10 - 1/25600 (self-titer).